Exciton Recombination in Formamidinium Lead Triiodide: Nanocrystals versus Thin Films

Author(s):
Fang, Hong-Hua; Protesescu, Loredana; Balazs, Daniel M.; Adjokatse, Sampson; Kovalenko, Maksym V.; Loi, Maria Antonietta

Publication date:
2017-08-25

Permanent link:
https://doi.org/10.3929/ethz-b-000191211

Originally published in:
Small 13(32), https://doi.org/10.1002/smll.201700673

Exciton Recombination in Formamidinium Lead Triiodide: Nanocrystals versus Thin Films

*Hong-Hua Fang, Loredana Protesescu, Daniel M. Balazs, Sampson Adjokatse, Maksym V. Kovalenko, and Maria Antonietta Loi**

The optical properties of the newly developed near-infrared emitting formamidinium lead triiodide ($FAPbI_3$) nanocrystals (NCs) and their polycrystalline thin film counterpart are comparatively investigated by means of steady-state and time-resolved photoluminescence. The excitonic emission is dominant in NC ensemble because of the localization of electron–hole pairs. A promisingly high quantum yield above 70%, and a large absorption cross-section (5.2×10^{-13} cm^{-2}) are measured. At high pump fluence, biexcitonic recombination is observed, featuring a slow recombination lifetime of 0.4 ns. In polycrystalline thin films, the quantum efficiency is limited by nonradiative trap-assisted recombination that turns to bimolecular at high pump fluences. From the temperature-dependent photoluminescence (PL) spectra, a phase transition is clearly observed in both NC ensemble and polycrystalline thin film. It is interesting to note that NC ensemble shows PL temperature antiquenching, in contrast to the strong PL quenching displayed by polycrystalline thin films. This difference is explained in terms of thermal activation of trapped carriers at the nanocrystal's surface, as opposed to the exciton thermal dissociation and trap-mediated recombination, which occur in thin films at higher temperatures.

1. Introduction

Lead halide perovskites have emerged as a new class of revolutionary semiconductors for various applications in optoelectronics, such as solar cells,[1–4] light-emitting diodes,[5] and lasers.[6] Perovskite thin films that can be prepared directly from solution have exhibited remarkable properties,[7,8] and impressive achievements in term of efficiency have brought perovskite solar cells in close competition with crystalline silicon photovoltaics.

In the last two years, the surge in development of halide perovskite nanocrystal has been motivated by the desire to take advantage of the nanoscale properties of these outstanding semiconductors.[9–14] Organic–inorganic hybrid perovskites adopt the general formula ABX_3, where A is an organic cation, B is a metal ion (such as Pb^{2+}, Sn^{2+}), and X is a halide anion.[15,16] An advantage of this family of materials is the wide range of compositional possibilities through substitutions to tailor their optoelectronic properties.[17] Kovalenko and co-workers explored cesium lead halide perovskites in the form of colloidal nanocrystals (NCs), whose emission spectra can be readily tuned over the entire visible spectral region by adjusting their composition (ratio of halides in mixed halide NCs) and by particle size (quantum-size effects).[9] Dong and co-workers have demonstrated a methylammonium cation version of the NCs ($CH_3NH_3PbX_3$) with photoluminescence efficiency up to 70%.[10] More recent works have shown the effectiveness of anion exchange reactions for compositional

Dr. H.-H. Fang, D. M. Balazs, S. Adjokatse, Prof. M. A. Loi
Photophysics & OptoElectronics
Zernike Institute for Advanced Materials
Nijenborgh 4, Groningen, 9747 AG, The Netherlands
E-mail: m.a.loi@rug.nl

Dr. L. Protesescu, Prof. M. V. Kovalenko
Department of Chemistry and Applied Biosciences
ETH Zürich
Vladimir Prelog Weg 1, Zürich 8093, Switzerland

Dr. L. Protesescu, Prof. M. V. Kovalenko
EMPA-Swiss Federal Laboratories for Materials Science and Technology
Überlandstrasse, 129, Dübendorf 8600, Switzerland

DOI: 10.1002/smll.201700673

fine-tuning of NCs.[18,19] Moreover, it has been suggested that perovskite nanostructures could exhibit enhanced photoluminescence properties and device performance; with them Cho et al. substantially increased the steady-state photoluminescence efficiency of $MAPbBr_3$ perovskite light-emitting diode.[5] Xiong and co-workers reported amorphous nanoparticle-based light-emitting diodes, showing an external quantum efficiency of up to 3.8%.[20]

Formamidinium lead triiodide in its 3D perovskite form is called α-$FAPbI_3$ or "black phase" and, especially in its Cs- and Br-doped variations, is one of the most popular materials for solar cell and lasing applications.[21–30] Compared with the archetypal but less-chemically durable—methylammonium lead triiodide ($MAPbI_3$) perovskite—it has a more symmetric crystal structure, absorption edge shifted toward the infrared and a better thermal stability. However, this desired α-$FAPbI_3$ tends to phase-transform into the wider bandgap, "yellow" δ-$FAPbI_3$, both in thin films and large single crystals.[31–33] Yang and co-workers reported that the color of $FAPbI_3$ crystals gradually changed from black to yellow, regardless of storage in the vacuum or inert gas.[34] Recently, the partial substitution of the FA cation has been reported to stabilize the perovskite phase of $FAPbI_3$.[35] However, this substitutional strategy also partially covers the properties of the $FAPbI_3$ material. Kovalenko and co-workers demonstrated that the black perovskite phase (α-$FAPbI_3$) in the form of colloidally synthesized NCs (10–15 nm, near cubic shape) exhibits improved phase-stability and shelf-life of at least six to nine months (see the Experimental Section and further details on the synthetic procedure in ref. [36]). This development opens avenues to investigate the optical properties of nanoscopic α-$FAPbI_3$ and to compare them with earlier studies on films and macroscopic single crystals.[15,37]

In this paper, we report transient and steady-state photoluminescence (PL) properties of the newly synthesized colloidal $FAPbI_3$ NCs and compare the results with the ones obtained for polycrystalline thin films. We show that the localization of photogenerated electron–hole pairs in $FAPbI_3$ NCs leads to a distinctly different landscape for the recombination of photoexcited carriers. Exciton recombination is dominant in NCs and exciton–exciton interactions come into play at escalated excitation intensities; while in the polycrystalline thin films, free carriers undergo trap assisted nonradiative recombination or bimolecular recombination, depending on the pump fluence.[38] For $FAPbI_3$ NCs, we measured an absorption cross-section as high as 5.2×10^{-13} cm^{-2}, PL quantum yield of about 70%, and a slow biexcitonic recombination lifetime of about 0.4 ns. The temperature dependent steady-state and time-resolved PL spectra are further investigated. Both NC ensembles and polycrystalline thin films show a phase transition at low temperature. Moreover, we observed a counterintuitive PL temperature antiquenching in ensemble of NCs, namely, the PL intensity increases with increasing temperature, while it significantly decreases in polycrystalline thin films. The PL dynamics and the underline recombination mechanisms are further discussed.

2. Results and Discussion

Figure 1a,b shows transmission electron microscopy images of $FAPbI_3$ NCs of size of about 13 ± 3 nm. The phase of α-$FAPbI_3$ (*Pm*-3*m*) was confirmed using powder X-ray diffraction (XRD) as shown in Figure S1 (Supporting Information). The UV–vis absorption and PL spectra of these NCs are shown in Figure 1c. The as-synthesized $FAPbI_3$ NCs in solution show emission at 782 nm (1.59 eV) with a very limited Stokes shift. Compared to the emission peak (823 nm) for the polycrystalline thin film, $FAPbI_3$ NCs result blue-shifted of about 41 nm, confirming their 3D confinement. The emission from NC ensembles deposited on quartz substrates shows about 6 nm red-shift respect to the solution spectrum, indicating that energy transfer occurs between NCs of different sizes. The NCs as-synthesized exhibit PL quantum yield (QY) as high as 70%; such high QY is remarkable given that these NCs are not protected with a shell of a wider bandgap semiconductor, and that they are

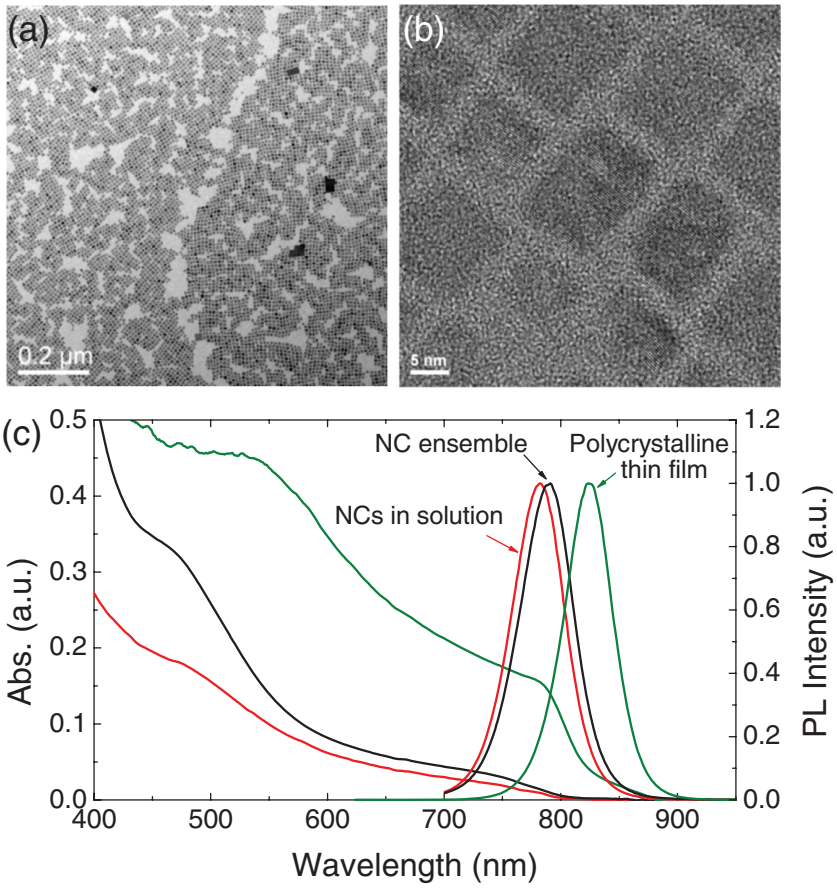

Figure 1. a) Large-area TEM image of $FAPbI_3$ NCs. b) A high-resolution TEM image of $FAPbI_3$ NCs. c) UV–vis absorption spectra and photoluminescence spectra of NCs in solution, ensemble, and polycrystalline thin film.

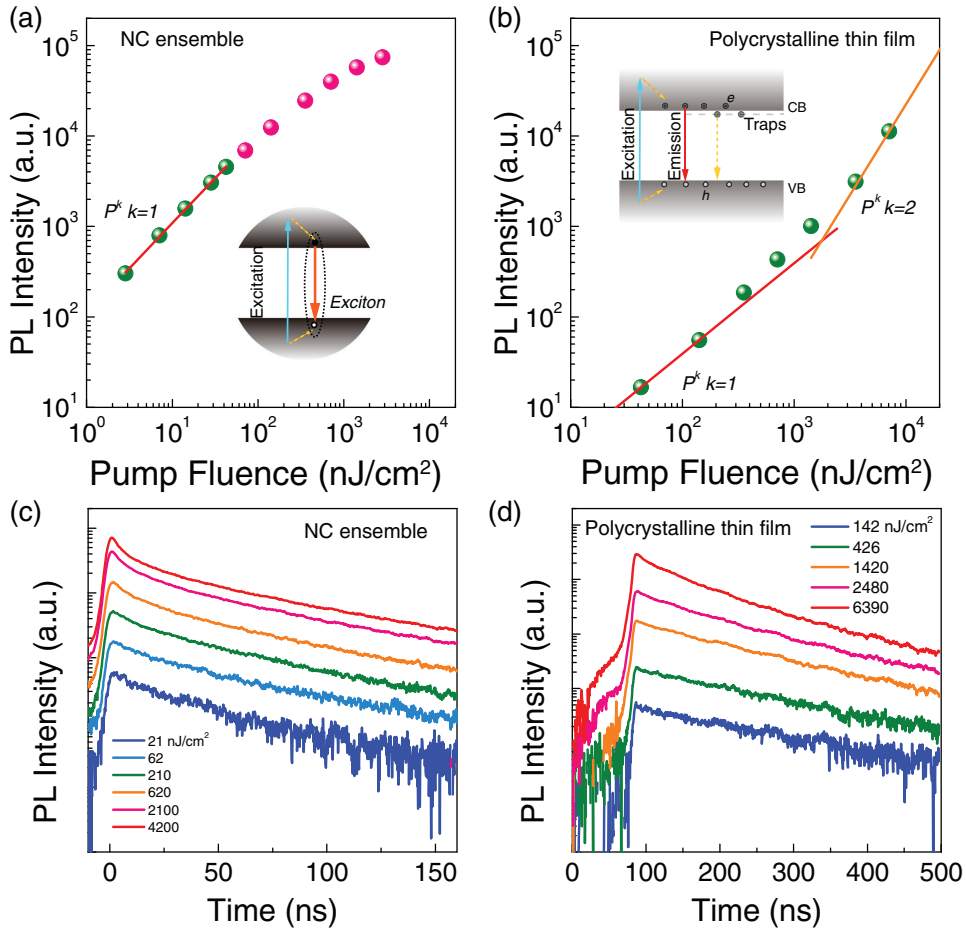

Figure 2. Photoluminescence intensity as a function of pump fluence for a) NC ensemble and b) polycrystalline thin film. PL decay at different excitation fluences for c) the NC ensemble and d) the polycrystalline thin film.

synthesized at relatively low temperatures. The high QY also suggests a considerably lower presence of intragap states in $FAPbI_3$ NCs respect to thin film, highlighting the excellent defect-tolerance properties of hybrid perovskites crystals.[39–42]

It is also noted that the PL QY of nanocrystal ensembles is about two-orders of magnitude higher than that of the thin films at low pump fluence (below 50 nJ cm^{-2}). This significant difference in emission intensity suggests different recombination processes. To determine which recombination processes dominate in our samples, we measured the PL spectra under various excitation densities for both NC ensembles and polycrystalline thin films (see Figures S2 and S3 of the Supporting Information). **Figure 2**a,b summarizes the PL intensity as a function of pump fluence in double-logarithmic scale for NC ensembles and polycrystalline thin films, respectively. Generally, the integrated PL intensity (I) is proportional to P^k, where P is the excitation fluence. The exponent k depends on the underlying radiative recombination process and is expected to be close to unity for monomolecular recombination, and around two in the case of bimolecular recombination of uncorrelated electron–hole pairs. In nanocrystal, the PL intensity increases linearly with pump fluence up to 100 nJ cm^{-2}, suggesting that the quantum yield in this range is constant. The slope becomes sublinear at higher excitation fluence. We attribute this slope variation to exciton–exciton interactions: biexcitonic recombinations appear at high pump fluence, as will be discussed later. In NCs, the photogenerated electrons and holes are confined because of their small size. The initial electron–hole pair population follows the Poisson distribution with the mean number per particle $\langle N\rangle = \sigma(h\nu) \times J_p(h\nu)$, where $J_p(h\nu)$ is the pump laser fluence and $\sigma(h\nu)$ is the average absorption cross-section of the NCs at the excitation wavelength.[43] The PL intensity is therefore proportional to (1-exp(−⟨N⟩)) (see the Supporting Information). Since the pump fluence J_p is a controllable parameter, the absorption cross-section σ can be reliably estimated. The derived equation fits the measured data well, as shown in Figure S4 of the Supporting Information. The absorption cross-section for $FAPbI_3$ NCs at 400 nm is quantified to be around 5.2×10^{-13} cm^{-2}, this value is very close to the cross-section estimated from the absorption spectra (2.6×10^{-13} cm^{-2}), and is very similar to the value (2.3×10^{-13} cm^2) measured in ensembles of $CsPbBr_3$ NCs by Xiao and co-workers,[44] confirming that $FAPbI_3$ NCs have inherited the excellent absorption capacity of bulk perovskites.

In the case of polycrystalline thin films, the PL intensity shows a linear dependence on the excitation power below 150 nJ cm^{-2} pump fluence. It increases superlinearly and follows a quadratic dependence at higher intensities (Figure 2b), indicating a different PL mechanism from that of the NC ensembles. This behavior is consistent with recent reports

about $MAPbI_3$ thin films,[45,46] showing that at low excitation levels (below 150 nJ cm^{-2}), the linear dependent PL intensity can be attributed to geminate and/or Shockley–Read–Hall mechanism (also called trap-assisted recombination).[47] Considering the low exciton binding energy (8.1 meV),[24] the possibility of geminate recombination is negligible at room temperature, therefore the recombination process is a trap-assisted recombination of free carriers. When the excitation is further increased, the trap states density approaches saturation. As shown in Figure 2b, the PL intensity is quadratically dependent on the pump fluence for excitations above 6390 nJ cm^{-2}. Therefore, the nongeminate bimolecular free electron–hole recombination becomes a dominant process at this excitation level.[47] These two regimes (trap-assisted recombination and bimolecular recombination) of light emission are identified clearly in the intensity dependent PL measurements (Figure 2b). The knowledge of the photocarrier density at the crossover point between the two regimes enables an approximate estimation of the defect density,[45,46] which is $\approx 8 \times 10^{16}$ cm^{-3} in our polycrystalline thin film.

To confirm the underlying recombination mechanism, the photoluminescence dynamics was investigated. Figure 2c,d reports the PL decays for the NC ensemble and thin film at their emission peaks under different pump fluences. With increasing excitation fluence, the decay in the NC ensemble shows an additional fast component with amplitude growing superlinearly with increasing excitation power. This is a typical signature of the formation of biexcitons due to fast nonradiative "Auger"-like processes. To validate that the measured signal comes from biexcitonic recombination, the measured PL decays are normalized to their long delay components, as shown in **Figure 3**a. Based on the Poisson distribution of the NC population, the PL should have a major contribution from single excitons and a small contribution from biexcitons in our experiment. The long delay PL decays are very similar for different excitation power, suggesting that they originate from the same species, specifically, single exciton recombination. The PL decay can be well described by a superposition of single exciton dynamics $f(t)$ and an additional single exponential biexciton component, $A \times \exp(-t/\tau_{BX}) + B \times f(t)$. Applying this fit, we obtain the biexciton recombination time to be 0.4 ns, which is much shorter than the measured single exciton lifetime (52 ns). This biexcitonic decay is much slower than that reported for $CsPbI_3$,[48] suggesting that these new NCs could have an application in lasing.[49] The PL intensity for the fast-decay component is obtained by subtracting the PL amplitude related to the slow-decay component at early time after photoexcitation. Figure 3c presents the power dependence of the fast-decay

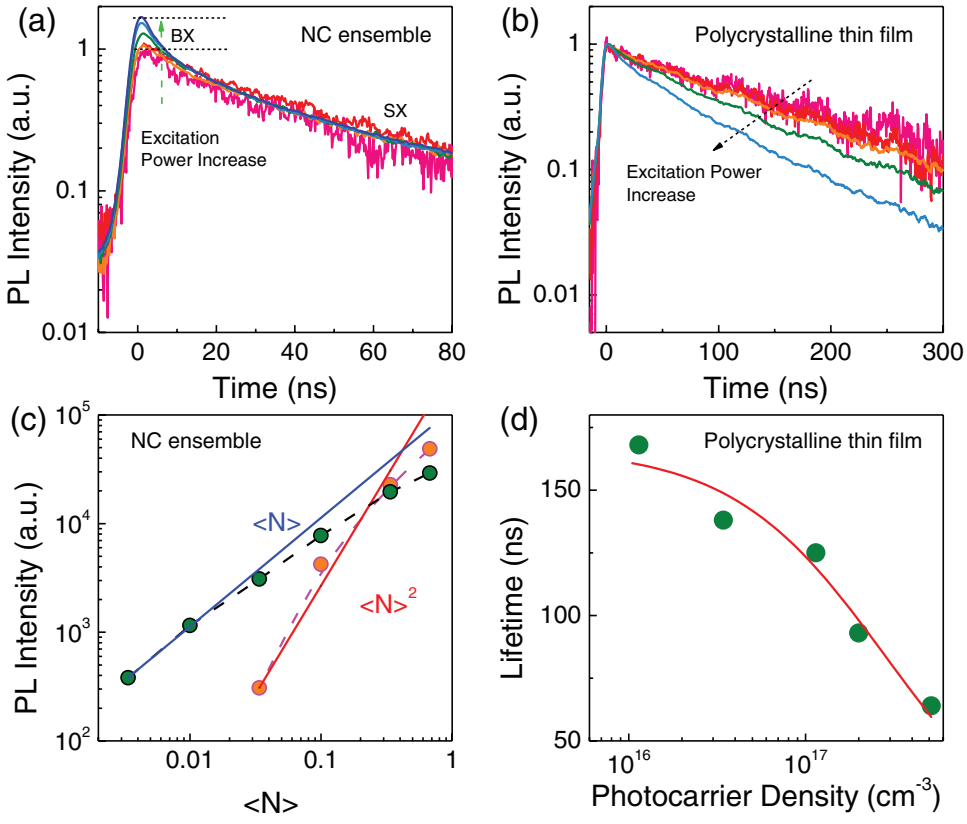

Figure 3. a) Excitation power-dependent PL dynamics of NC ensemble. The PL decays are normalized to match the late-time tails, which correspond to the single-exciton recombination. The early time short-lived PL components at high excitation power show biexciton recombination. b) Normalized power-dependent PL dynamics from $FAPbI_3$ films. c) Excitation power-dependence of the single-exciton PL amplitude and the amplitude of the biexcitonic component follow the expected trends obtained assuming Poisson statistics of the initial NC occupancies (solid lines). The early time short-lived PL component follows the quadratic scaling, as expected for biexcitons (red dashed line). d) Excitation-intensity dependence of the effective PL lifetime of the polycrystalline film. The red line is obtained from the fitting $\frac{1}{\tau} = A + Bn_0$, where τ is the effective lifetime, n_0 is the initial PL intensity after excitation, A and B are constants.

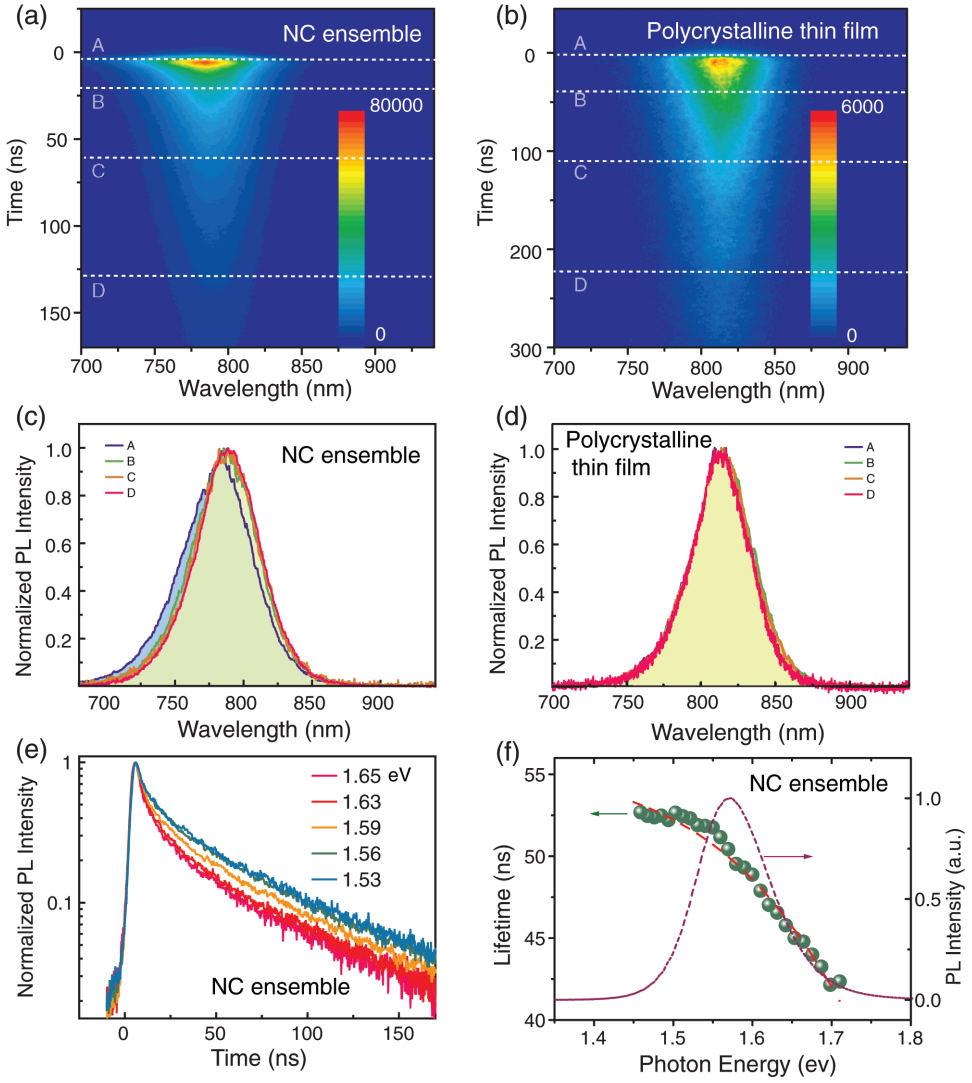

Figure 4. 2D pseudocolor plot as obtained from the streak camera of a) ensemble of $FAPbI_3$ NCs, and b) polycrystalline thin film. c,d) PL spectra extracted at different delays after excitation as indicated in (a) and (b) for the NC ensemble, and the polycrystalline thin film, respectively. e) PL decay times monitored at various emission energies for the ensemble NCs. f) Lifetimes as a function of emission energy, as well as time-integrated PL spectra taken under 4.1 μJ cm^{-2} excitation. The lifetimes decrease on the high-energy side of the emission. The red dashed line is the fitting performed using Equation (1).

component, as well as the single exciton contribution, which is extracted from the long-delay signal after the fast-initial decay. The amplitude of the fast decay component in the $\langle N \rangle$ range between 0.03 and 0.3 approximately scales as $\langle N \rangle^2$, confirming that it is indeed due to biexciton recombination.

The power-dependent decay in polycrystalline thin films is significantly different from the one of the NC ensemble. Figure 3d shows that the PL lifetime decreases as the excitation fluence increases in thin films. As previously presented, the charge carrier relaxation dynamics in bulk perovskite can be described as a function of the charge carrier density (n):[45,50] $-dn/dt = An + Bn^2$, where A and B are constants. The linear term describes the monomolecular recombination, which arises from charge trapping, the quadratic term accounts for the bimolecular recombination. By fitting the PL dynamics with the rate equation, we obtained values $A = 6 \times 10^6$ s^{-1}, and $B = 0.21 \times 10^{-10}$ s^{-1} cm^3, which are in line with recently reported values for hybrid perovskites.[45,50]

Therefore, it is clear that different recombination processes are observed in $FAPbI_3$ polycrystalline thin film and NC ensembles. Difference that is attributed to the localization of electron–hole pairs in NCs.[51] Due to their small volume, the photogenerated carriers in NCs are spatially confined and their exciton dissociation probability becomes negligible. This consequently increases the possibility of radiative recombination in NCs compared with polycrystalline thin film.

As discussed previously, excitons in $FAPbI_3$ NC are localized by their size confinement, however, communication and coupling between these localized states may occur in ensembles. In this case, the excitons tend to migrate toward lower energy sites.[52,53] To investigate if such a migration is occurring, we recorded the spectrally resolved photoluminescence dynamics. The 2D contour plot of the time-resolved PL spectra of the $FAPbI_3$ NC ensemble is presented in **Figure 4**a, while the one for the $FAPbI_3$ polycrystalline thin film is presented in Figure 4b for comparison. Figure 4c,d shows the extracted PL

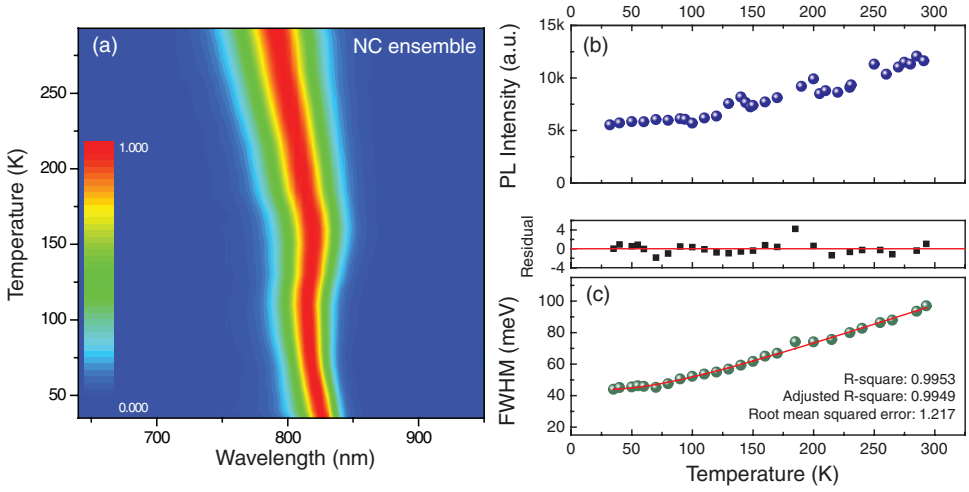

Figure 5. a) Normalized emission spectra of the NC ensemble excited with a pump power density of 70 nJ cm^{-2} at different temperatures. b) Temperature-dependent integrated PL intensity, showing the temperature antiquenching of the PL. c) Full width at half maximum (FWHM) of the PL spectra as a function of the temperature. The red solid line is the result of a fit using Equation (2), including contributions from inhomogeneous broadening, acoustic and optical phonons.

spectra at specified times after the excitation. The clear difference is that the emission peak red-shifts in the $FAPbI_3$ NC ensemble, while remains constant with time in the thin film. In the NC ensemble, the emission red-shifts in the first 10 ns, to remain roughly constant at 788 nm beyond 30 ns, demonstrating the energy transfer between particles of slightly different sizes. As a result of energy transfer, the PL lifetime is strongly dependent on the emission energy in NC ensembles. Figure 4e shows the room temperature PL decays extracted at different excitation energies. The PL lifetimes decrease with increasing emission energy; the PL decay times as a function of the monitored emission energy, together with the time integrated spectrum are reported in Figure 4f. As already mentioned the spectral dependence of the lifetime is due to the migration process to the tail states in the NC ensemble, as observed in conventional quantum dot solids.[54] If the tail state distribution is approximated as $\exp(-E/E_0)$, then the lifetime at different emission energies can be expressed as:[55]

$$\tau_e = \frac{\tau_0}{1+e^{\frac{E-E_{me}}{E_0}}} \quad (1)$$

where τ_0 is the lifetime of localized excitons, E_{me} is the energy for which the radiative lifetime equals the lateral transfer time, and E_0 is a characteristic energy of the density of band tail states, which is a measure of the average localization energy. Above E_{me}, the transfer of excitons has a higher probability than the radiative decay. Applying Equation (1) (red dotted line in Figure 4f) yields a radiative lifetime of $\tau_0 = 57$ ns, $E_{me} = 1.84$ eV and $E_0 = 124$ meV. The large E_{me} suggests that the PL decay from NC ensembles is dominated by recombination of localized excitons.

The PL lifetime of the polycrystalline thin films is practically independent of the wavelength at room temperature (Figure 4a). This spectrally stable PL decay is a further evidence of the fact that the photoluminescence is governed by band to band transitions.[24]

The photophysical properties of hybrid perovskites have been shown to be highly temperature-dependent.[15,24,56,57] **Figure 5**a displays a 2D pseudocolor plot of the normalized PL spectra of the NC ensemble as a function of temperature. A clear evolution in the peak position can be observed, with the spectrum monotonously red-shifting from room temperature to ≈150 K, followed by a sudden blue-shift between 150 and 120 K, back to a shift toward lower energy at temperatures lower than 120 K, which is similar to the behavior observed in microstructures of $FAPbBr_3$.[58] This abrupt PL shift is likely due to the bandgap shift imposed by the thermal expansion and change of the in-plane lattice constants during the crystallographic phase transition, which is occurring in the bulk around 140 K from the β tetragonal phase ($P3$) to the γ orthorhombic phase ($Pnma$) (Figure S4, Supporting Information).[59,60] The monotonous shift for the high-temperature phase can be described by a temperature coefficient $\alpha = \partial E/\partial T = 0.43$ meV K^{-1} for the NC ensemble (Figure S4, Supporting Information), which is slightly larger than the value $\alpha = 0.39$ meV K^{-1} reported for the polycrystalline thin film, suggesting a larger thermal expansion in NCs, which is not unexpected for nanometer-sized crystals.

Figure 5b reports the integrated PL intensity as a function of temperature. In the polycrystalline thin film, strong thermal quenching of the photoluminescence intensity is observed,[24] with the PL intensity at room temperature being only the 5% of the value at 5 K (see Figure S6 of the Supporting Information). The thermal quenching in the polycrystalline thin film is attributed to thermal dissociation of excitons at high temperature and phonon interactions. By contrast, the PL intensities of the NC ensemble show an antiquenching behavior with increasing temperature. The PL intensity at room temperature is about three times higher than at 35 K. This antiquenching behavior suggests again different recombination mechanism in NC ensemble respect to the one in polycrystalline films.

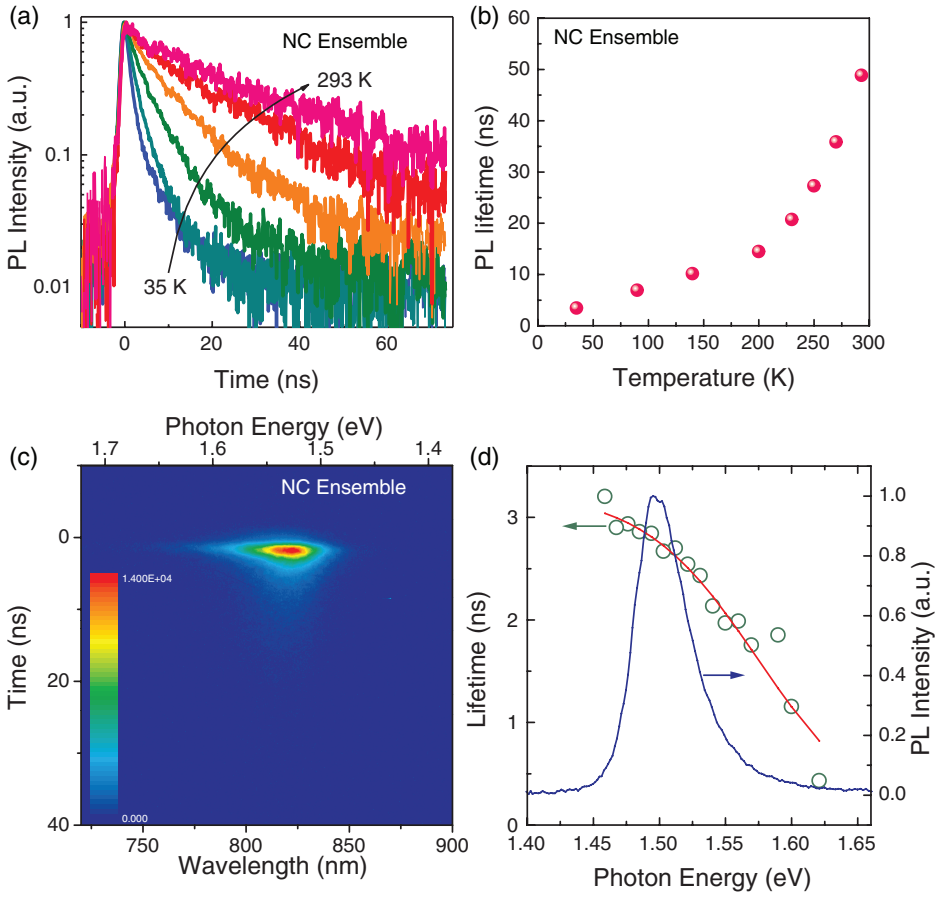

Figure 6. a) Normalized PL decays of the NC ensemble under a pump fluence of 70 nJ cm^{-2} at different temperatures. b) Temperature-dependent PL lifetimes showing a decrease at low temperature. c) 2D pseudocolor plot of streak camera data of the NC ensemble at 35 K. d) Lifetimes as a function of emission energy, as well as the time-integrated PL taken at 35 K.

The exciton–phonon coupling in NC ensembles was studied by analyzing the temperature dependent emission linewidth broadening, which increases from 44 to 97 meV with increasing of the temperature from 35 to 295 K (Figure 5c). The temperature-dependent emission linewidth due to exciton–phonon coupling can be described by the following classical equation:[61]

$$\Gamma(T) = \Gamma_{\text{inh}} + \sigma T + \Gamma_{\text{LO}}/(\exp(h\omega_{\text{o}}/k_{\text{B}}T) - 1) \quad (2)$$

Here, Γ_{inh} is the inhomogeneous broadening contribution, which arises from scattering due to disorder and imperfections, σ and Γ_{LO} are the exciton–acoustic phonons and the exciton–optical phonon coupling coefficients, respectively, $h\omega_{\text{o}}$ is the optical phonon energy, and k_{B} is the Boltzmann constant. From the best fit performed with this equation, we found that the inhomogeneous broadening is 43 meV for the NC ensemble, which is noticeably larger than the one measured for polycrystalline thin films (18 meV). The larger broadening can be attributed to the effect of polydispersity, and the subsequent energy level disorder in the NC ensemble (see the time-dependent PL peak position shift). The optical phonon energy in NC ensembles is estimated to be 19 meV, which is very close to the value obtained for the $FAPbI_3$ polycrystalline thin films (18 meV). This suggests a similar contribution of the Fröhlich interaction between charge carriers and optical phonons in homogeneous linewidth broadening in NC ensembles and polycrystalline thin films at room temperature.[61]

To understand the temperature dependent recombination mechanism, the time-resolved PL at different temperatures was investigated (see **Figure 6**a). In the low-temperature range, the PL decays can be fitted with biexponential functions. In Figure 6b, the average lifetime determined from the decays are plotted as a function of temperature. As the temperature is raised, the decay time in NC ensembles becomes longer. This trend further confirms the unusual PL temperature antiquenching effect in these NC ensembles. We conjecture that an optically dark state is present in the $FAPbI_3$ NC, which lies energetically below the emissive exciton state. The origin of this dark state is likely correlated with a surface state, in which one of the charge carriers is trapped. The state is preferentially populated at a low temperature, and thus reduces the population of emissive excited states, and decreases the corresponding PL intensity, as well as the lifetime. Similar phenomena were observed in CdSe-core CdS/CdZnS/ZnS-multishell quantum dots.[62] Figure 6c presents the spectrally and temporally resolved photoluminescence

measurements of NC ensembles at 35 K. The lifetime as a function of emission energy at 35 K, as well as time-integrated PL, are shown in Figure 6d. The emission energy dependence of the lifetime can be attributed to the exciton migration toward tail states in the NC ensemble, as previously discussed for the room temperature measurements, obviously at low temperature the energy transfer is less efficient.[53]

It is very interesting to compare the low-temperature PL in NC ensembles with their polycrystalline thin films counterpart. In the latter, the emission peak is around 860 nm at 30 K, with a low energy shoulder (see Figure S7 of the Supporting Information). The shoulder emission exhibits a long lifetime up 2 μs, this long-lived component is attributed to the radiative recombination of bound excitons (X_B) that are formed by localizing excitons at defect sites, as observed in $MAPbI_3$ crystals, and $FAPbI_3$ thin films.[15,24] With increasing pump fluence, the PL intensity of X_B is expected to saturate at high excitation power intensities when these defects are fully populated with excitons. This is indeed confirmed by power-dependent photoluminescence measurements reported in Figure S8 of the Supporting Information.[15] In the NC ensembles, we did not observe such radiative recombination from a bound exciton, and the normalized PL spectra measured with different pump intensity are identical, with a slightly broader full width at half maximum at higher pump fluence (Figure S9, Supporting Information). As already mentioned, the photoexcitation dynamics in NC ensembles also show a significant difference from their polycrystalline thin film counterpart (see Figure S10 of the Supporting Information). The PL lifetime of NC ensembles at 30 K is around 3 ns, which is three orders of magnitude shorter than that observed in thin films. As discussed above the much shorter lifetime of the NC sample is interpreted as due to shallow trap states, localized at the NC surface.

3. Conclusion

In conclusion, we have investigated the photoexcitation recombination dynamics in $FAPbI_3$ nanocrystal ensembles in comparison with polycrystalline thin films at various temperatures. The recombination processes in NC ensembles display a very different nature respect to their polycrystalline thin film counterpart. At room temperature, the excitonic emission is dominant in NC ensembles, with a high photoluminescence quantum yield of up to 70%, which is about two orders of magnitude higher than that of thin films. The NCs exhibit a large absorption cross-section of 5.2×10^{-13} cm^{-2} at 400 nm. With increasing pump fluence, we observed a relatively slow biexciton emission, with recombination time of 0.4 ns, demonstrating the potential for the lasing of these newly synthesized NCs. On the other hand, in polycrystalline thin films, trap-assistant recombination plays an important role at low pump fluence; while bimolecular recombination dominates the photoluminescence at elevated excitation powers. From the temperature-dependent PL spectra, a phase transition is clearly observed in both NC ensembles and polycrystalline thin films. In contrast to the observed strong thermal PL quenching observed in the polycrystalline thin films, NC ensembles show PL temperature antiquenching. This behavior is explained by thermal activation of trapped excitons at the NC surface with increasing temperature, while radiative recombination of bound excitons is observed at low temperatures in the polycrystalline thin films. Our results provide insights into the charge recombination mechanism in NC ensembles and polycrystalline thin films and help to unravel their potential for high-performance optoelectronic devices.

4. Experimental Section

Materials: The NCs of $FAPbI_3$ were synthesized using the following procedure: $Pb(acetate)_2 \times 3H_2O$ (0.076 g, 0.2 mmol, Aldrich, *99.99%*), FA-acetate (0.078 g, 0.75 mmol), 1-octadenece (ODE) (6 mL, dried), and oleic acid (OA) (4 mL, dried) were combined in a 25 mL three-neck flask and dried under vacuum for 30 min at 50 °C. The mixture was heated to 80 °C under N_2, followed by the injection of oleylammonium idoide (OAmI) (0.237 g, 0.6 mmol in 2 mL toluene; the OAmI was prepared according to literature).[18] After 10 s, the reaction mixture was cooled in a water bath. The crude solution was centrifuged for 5 min at 12 100 rpm, the supernatant was discarded, and the precipitate was redispersed in toluene and washed two times with acetonitrile (3:1 toluene:acetonitrile) and dispersed in chloroform for processing. The solution was drop casted or spin-coated on a quartz substrate to form a NC ensemble for optical characterization.

Perovskite polycrystalline thin films were prepared according to a previous report.[24] FAI and PbI_2 were dissolved in anhydrous *N*,*N*-dimethylformamide at a molar ratio of 1:1. 5 vol% and hydriodic acid was added to the mixed solution. The precursor solution was spin-coated at 3000 rpm for 60 s on a fluorine-doped tin oxide (FTO) coated glass substrate and then dried at 160 °C for 30 min.

Powder X-ray diffraction (XRD) patterns were performed using a STOE STADI P diffractometer, operating in transmission mode. A germanium monochromator, Cu Kα1 irradiation and a silicon strip detector (Dectris Mythen) were used.

Spectroscopic Measurements: All samples were photoexcited with 3.1 eV photons. The laser power was adjusted using neutral density filters. The excitation beam was spatially limited by an iris and focused with a 150 mm focal length lens. Emitted photons were collected with a lens and directed to a spectrograph. For time-resolved PL measurements, a pulse picker was used to reduce the Ti:sapphire oscillator frequency (about 76 MHz). Steady-state spectra were collected using a Hamamatsu EM-CCD camera and time resolved traces were recorded using a Hamamatsu streak camera working in single sweep mode. For low temperature measurements, samples were installed in a liquid helium optical cryostat (Oxford Optistat). The room temperature UV–vis absorption spectra were measured with a Shimadzu UV3000 spectrometer.

Supporting Information

Supporting Information is available from the Wiley Online Library or from the author.

Acknowledgements

The authors would like to thank Arjen Kamp and Theodor Zaharia for the technical support. The Groningen team is grateful for the financial support of the European Research Council (ERC Starting Grant "Hy-SPOD" No. 306983). M.V.K. acknowledges financial support from the European Union through the FP7 (ERC Starting Grant NANOSOLID, GA No. 306733) and in part from the Swiss Federal Commission for Technology and Innovation (CTI-No. 18614.1 PFNM-NM).

Conflict of Interest

The authors declare no conflict of interest.

[1] M. Liu, M. B. Johnston, H. J. Snaith, *Nature* **2013**, *501*, 395.
[2] S. Shao, Z. Chen, H.-H. Fang, G. H. ten Brink, D. Bartesaghi, S. Adjokatse, L. J. A. Koster, B. J. Kooi, A. Facchetti, M. A. Loi, *J. Mater. Chem. A* **2016**, *4*, 2419.
[3] M. A. Green, A. Ho-Baillie, H. J. Snaith, *Nat. Photonics* **2014**, *8*, 506.
[4] N. Pellet, P. Gao, G. Gregori, T. Y. Yang, M. K. Nazeeruddin, J. Maier, M. Grätzel, *Angew. Chem. Int. Ed.* **2014**, *53*, 3151.
[5] H. Cho, S.-H. Jeong, M.-H. Park, Y.-H. Kim, C. Wolf, C.-L. Lee, J. H. Heo, A. Sadhanala, N. Myoung, S. Yoo, S. H. Im, R. H. Friend, T.-W. Lee, *Science* **2015**, *350*, 1222.
[6] H. Zhu, Y. Fu, F. Meng, X. Wu, Z. Gong, Q. Ding, M. V Gustafsson, M. T. Trinh, S. Jin, X.-Y. Zhu, *Nat. Mater.* **2015**, *14*, 636.
[7] H.-H. Fang, S. Adjokatse, H. Wei, J. Yang, G. R. Blake, J. Huang, J. Even, M. A. Loi, *Sci. Adv.* **2016**, *2*, 1.
[8] J. S. Manser, J. A. Christians, P. V. Kamat, *Chem. Rev.* **2016**, *116*, 12956.
[9] L. Protesescu, S. Yakunin, M. I. Bodnarchuk, F. Krieg, R. Caputo, C. H. Hendon, R. X. Yang, A. Walsh, M. V. Kovalenko, *Nano Lett.* **2015**, *15*, 3692.
[10] F. Zhang, H. Zhong, C. Chen, X. G. Wu, X. Hu, H. Huang, J. Han, B. Zou, Y. Dong, *ACS Nano* **2015**, *9*, 4533.
[11] X. Zhang, H. Lin, H. Huang, C. Reckmeier, Y. Zhang, W. C. H. Choy, A. L. Rogach, *Nano Lett.* **2016**, *16*, 1415.
[12] O. Vybornyi, S. Yakunin, M. V Kovalenko, *Nanoscale* **2016**, *8*, 6278.
[13] L. C. Schmidt, A. Pertegás, S. González-Carrero, O. Malinkiewicz, S. Agouram, G. Mínguez Espallargas, H. J. Bolink, R. E. Galian, J. Pérez-Prieto, *J. Am. Chem. Soc.* **2014**, *136*, 850.
[14] M. E. Kamminga, H.-H. Fang, M. R. Filip, F. Giustino, J. Baas, G. R. Blake, M. A. Loi, T. T. M. Palstra, *Chem. Mater.* **2016**, *28*, 4554.
[15] H.-H. Fang, R. Raissa, M. Abdu-Aguye, S. Adjokatse, G. R. Blake, J. Even, M. A. Loi, *Adv. Funct. Mater.* **2015**, *25*, 2378.
[16] I. Borriello, G. Cantele, D. Ninno, *Phys. Rev. B* **2008**, *77*, 235214.
[17] A. Amat, E. Mosconi, E. Ronca, C. Quarti, P. Umari, M. K. Nazeeruddin, M. Grätzel, F. De Angelis, *Nano Lett.* **2014**, *14*, 3608.
[18] G. Nedelcu, L. Protesescu, S. Yakunin, M. I. Bodnarchuk, M. J. Grotevent, M. V. Kovalenko, *Nano Lett.* **2015**, *15*, 5635.
[19] D. Zhang, Y. Yang, Y. Bekenstein, Y. Yu, N. A. Gibson, A. B. Wong, S. W. Eaton, N. Kornienko, Q. Kong, M. Lai, A. P. Alivisatos, S. R. Leone, P. Yang, *J. Am. Chem. Soc.*, **2016**, *138*, 7236.
[20] J. Xing, F. Yan, Y. Zhao, S. Chen, H. Yu, Q. Zhang, R. Zeng, H. V. Demir, X. Sun, A. Huan, Q. Xiong, *ACS Nano* **2016**, *10*, 6623.
[21] G. E. Eperon, S. D. Stranks, C. Menelaou, M. B. Johnston, L. M. Herz, H. J. Snaith, *Energy Environ. Sci.* **2014**, *7*, 982.
[22] H.-H. Fang, F. Wang, S. Adjokatse, N. Zhao, M. A. Loi, *Adv. Funct. Mater.* **2016**, *26*, 4653.
[23] W. S. Yang, J. H. Noh, N. J. Jeon, Y. C. Kim, S. Ryu, J. Seo, S. Il Seok, *Science* **2015**, *348*, 1234.
[24] H.-H. Fang, F. Wang, S. Adjokatse, N. Zhao, J. Even, M. A. Loi, *Light: Sci. Appl.* **2016**, *5*, e16056.
[25] D. Bi, W. Tress, M. I. Dar, P. Gao, J. Luo, C. Renevier, K. Schenk, A. Abate, F. Giordano, J.-P. Correa Baena, J.-D. Decoppet, S. M. Zakeeruddin, M. K. Nazeeruddin, M. Grätzel, A. Hagfeldt, *Sci. Adv.* **2016**, *2*, e1501170.
[26] N. J. Jeon, J. H. Noh, W. S. Yang, Y. C. Kim, S. Ryu, J. Seo, S. Il Seok, *Nature* **2015**, *517*, 476.
[27] S. Yang, Y. Wang, P. Liu, Y.-B. Cheng, H. J. Zhao, H. G. Yang, *Nat. Energy* **2016**, *1*, 15016.
[28] F. Wang, W. Geng, Y. Zhou, H.-H. Fang, C. Tong, M. A. Loi, L.-M. Liu, N. Zhao, *Adv. Mater.* **2016**, *28*, 9986.
[29] M. T. Weller, O. J. Weber, J. M. Frost, A. Walsh, *J. Phys. Chem. Lett.* **2015**, *6*, 3209.
[30] Y. Fu, H. Zhu, A. W. Schrader, D. Liang, Q. Ding, P. Joshi, L. Hwang, X.-Y. Zhu, S. Jin, *Nano Lett.* **2016**, *16*, 1000.
[31] M. I. Saidaminov, A. L. Abdelhady, G. Maculan, O. M. Bakr, *Chem. Commun.* **2015**, *51*, 17658.
[32] Z. Wang, Y. Zhou, S. Pang, Z. Xiao, J. Zhang, W. Chai, H. Xu, Z. Liu, N. P. Padture, G. Cui, *Chem. Mater.* **2015**, *27*, 7149.
[33] A. Binek, F. C. Hanusch, P. Docampo, T. Bein, *J. Phys. Chem. Lett.* **2015**, *6*, 1249.
[34] Q. Han, S.-H. Bae, P. Sun, Y.-T. Hsieh, Y. M. Yang, Y. S. Rim, H. Zhao, Q. Chen, W. Shi, G. Li, Y. Yang, *Adv. Mater.* **2016**, *28*, 2253.
[35] J. Dai, Y. Fu, L. H. Manger, M. T. Rea, L. Hwang, R. H. Goldsmith, S. Jin, *J. Phys. Chem. Lett.* **2016**, *7*, 5036.
[36] L. Protesescu, S. Yakunin, S. Kumar, J. Bär, F. Bertolotti, N. Masciocchi, A. Guagliardi, M. Grotevent, I. Shorubalko, M. I. Bodnarchuk, C.-J. Shih, M. V. Kovalenko, *ACS Nano* **2017**, *11*, 3119.
[37] P. Piatkowski, B. Cohen, C. S. Ponseca, M. Salado, S. Kazim, S. Ahmad, V. Sundström, A. Douhal, *J. Phys. Chem. Lett.* **2016**, *7*, 204.
[38] P. Piatkowski, B. Cohen, S. Kazim, S. Ahmad, A. Douhal, *Phys. Chem. Chem. Phys.* **2016**, *18*, 27090.
[39] W.-J. Yin, T. Shi, Y. Yan, *Appl. Phys. Lett.* **2014**, *104*, 63903.
[40] D. N. Dirin, L. Protesescu, D. Trummer, I. V. Kochetygov, S. Yakunin, F. Krumeich, N. P. Stadie, M. V. Kovalenko, *Nano Lett.* **2016**, *16*, 5866.
[41] M. I. Saidaminov, J. Almutlaq, S. Sarmah, I. Dursun, A. A. Zhumekenov, R. Begum, J. Pan, N. Cho, O. F. Mohammed, O. M. Bakr, *ACS Energy Lett.* **2016**, *1*, 840.
[42] R. E. Brandt, V. Stevanović, D. S. Ginley, T. Buonassisi, *MRS Commun.* **2015**, *5*, 265.
[43] V. I. Klimov, *J. Phys. Chem. B* **2000**, *104*, 6112.
[44] F. Hu, H. Zhang, C. Sun, C. Yin, B. Lv, C. Zhang, W. W. Yu, X. Wang, Y. Zhang, M. Xiao, *ACS Nano* **2015**, *9*, 12410.
[45] Y. Yamada, T. Nakamura, M. Endo, A. Wakamiya, Y. Kanemitsu, *J. Am. Chem. Soc.* **2014**, *136*, 11610.
[46] J. Blancon, W. Nie, A. J. Neukirch, G. Gupta, S. Tretiak, L. Cognet, A. D. Mohite, J. J. Crochet, *Adv. Funct. Mater.* **2016**, *26*, 4283.
[47] L. H. Manger, M. B. Rowley, Y. Fu, A. K. Foote, M. T. Rea, S. L. Wood, S. Jin, J. C. Wright, R. H. Goldsmith, *J. Phys. Chem. C* **2017**, *121*, 1062.
[48] Y.-S. Park, S. Guo, N. S. Makarov, V. I. Klimov, *Nano Lett.* **2015**, *9*, 10386.
[49] J. Q. Grim, S. Christodoulou, F. Di Stasio, R. Krahne, R. Cingolani, L. Manna, I. Moreels, *Nat. Nanotechnol.* **2014**, *9*, 891.

[50] W. Rehman, R. L. Milot, G. E. Eperon, C. Wehrenfennig, J. L. Boland, H. J. Snaith, M. B. Johnston, L. M. Herz, *Adv. Mater.* **2015**, *27*, 7938.
[51] K. Zheng, Q. Zhu, M. Abdellah, M. E. Messing, W. Zhang, A. Generalov, Y. Niu, L. Ribaud, S. E. Canton, T. Pullerits, *J. Phys. Chem. Lett.* **2015**, *6*, 2969.
[52] S. A. Crooker, J. A. Hollingsworth, S. Tretiak, V. I. Klimov, *Phys. Rev. Lett.* **2002**, *89*, 186802.
[53] L. V. Poulikakos, F. Prins, W. A. Tisdale, *J. Phys. Chem. C* **2014**, *118*, 7894.
[54] H.-H. Fang, D. M. Balazs, L. Protesescu, M. V. Kovalenko, M. A. Loi, *J. Phys. Chem. C* **2015**, *119*, 17480.
[55] T. Bartel, M. Dworzak, M. Strassburg, A. Hoffmann, A. Strittmatter, D. Bimberg, *Appl. Phys. Lett.* **2004**, *85*, 1946.
[56] K. Wei, Z. Xu, R. Chen, C. Shen, X. Cheng, T. Jiang, *Opt. Lett.* **2016**, *41*, 3821.
[57] R. L. Milot, G. E. Eperon, H. J. Snaith, M. B. Johnston, L. M. Herz, *Adv. Funct. Mater.* **2015**, *25*, 6218.
[58] J. Dai, H. Zheng, C. Zhu, J. Lu, C. Xu, *J. Mater. Chem. C* **2016**, *4*, 4408.
[59] C. C. Stoumpos, C. D. Malliakas, M. G. Kanatzidis, *Inorg. Chem.* **2013**, *52*, 9019.
[60] D. H. Fabini, C. C. Stoumpos, G. Laurita, A. Kaltzoglou, A. G. Kontos, P. Falaras, M. G. Kanatzidis, R. Seshadri, *Angew. Chem. Int. Ed.* **2016**, *55*, 15392.
[61] A. D. Wright, C. Verdi, R. L. Milot, G. E. Eperon, M. A. Pérez-Osorio, H. J. Snaith, F. Giustino, M. B. Johnston, L. M. Herz, *Nat. Commun.* **2016**, *7*, 11755.
[62] P. Jing, J. Zheng, M. Ikezawa, X. Liu, S. Lv, X. Kong, J. Zhao, Y. Masumoto, *J. Phys. Chem. C* **2009**, *113*, 13545.

Received: February 28, 2017
Revised: April 16, 2017
Published online: June 22, 2017

